2017

Recent Land Cover Changes and Sensitivity of the Model Simulations to Various Land Cover Datasets for China

Rezaul Mahmood
University of Nebraska - Lincoln

Meteorol Atmos Phys (2017) 129:395–408
DOI 10.1007/s00703-016-0478-5

ORIGINAL PAPER

Recent land cover changes and sensitivity of the model simulations to various land cover datasets for China

Liang Chen[1,4] · Zhuguo Ma[1] · Rezaul Mahmood[2] · Tianbao Zhao[1] · Zhenhua Li[3] · Yanping Li[4]

Received: 13 November 2015 / Accepted: 7 September 2016 / Published online: 13 September 2016

Abstract Reliable land cover data are important for improving numerical simulation by regional climate model, because the land surface properties directly affect climate simulation by partitioning of energy, water and momentum fluxes and by determining temperature and moisture at the interface between the land surface and atmosphere. China has experienced significant land cover change in recent decades and accurate representation of these changes is, hence, essential. In this study, we used a climate model to examine the changes experienced in the regional climate because of the different land cover data in recent decades. Three sets of experiments are performed using the same settings, except for the land use/cover (LC) data for the years 1990, 2000, 2009, and the model default LC data. Three warm season periods are selected, which represented a wet (1998), normal (2000) and a dry year (2011) for China in each set of experiment. The results show that all three sets of land cover experiments simulate a warm bias relative to the control with default LC data for near-surface temperature in summertime in most parts of China. It is especially noticeable in the southwest China and south of the Yangtze River, where significant changes of LC occurred. Deforestation in southwest China and to the south of Yangtze River in the experiment cases may have contributed to the negative precipitation bias relative to the control cases. Large LC changes in northwestern Tibetan Plateau for 2000 and 2009 datasets are also associated with changes in surface temperature, precipitation, and heat fluxes. Wind anomalies and energy budget changes are consistent with the precipitation and temperature changes.

Responsible Editor: X.-Y. Huang.

✉ Liang Chen
chenliang@tea.ac.cn

[1] Key Laboratory of Regional Climate Environment for Temperate East Asia, Institute of Atmospheric Physics, Chinese Academy of Sciences, 40#Hua Yan Li, Qi Jia Huo Zi, Chao Yang District, Beijing 100029, China

[2] Department of Geography and Geology and Kentucky Climate Center, Western Kentucky University, Bowling Green, KY, USA

[3] Institute of Space and Atmospheric Studies, University of Saskatchewan, Saskatoon, SK, Canada

[4] Global Institute of Water Security, University of Saskatchewan, Saskatoon, SK, Canada

1 Introduction

Recent literature clearly illustrates the important role that land cover plays in land–surface interactions. It has been shown that the state of the land cover can impact convective system development, atmospheric circulation, regional-scale moisture fluxes, precipitation, and temperature (Barlage and Zeng 2004; Beljaars et al. 1996; Chang and Wetzel 1991; Chen and Avissar 1994; Clark and Arritt 1995; Mahmood and Hubbard 2002; Mahmood et al. 2010, 2011, 2014; McPherson 2007; Ookouchi et al. 1984; Pielke 2001). As a result, it is expected that land cover changes (LCC) would also modify the existing characteristics of land–surface atmosphere interactions and weather and climate. Many regional and large-scale studies support this understanding (e.g., Abiodun et al. 2008; Beltrán-Przekurat et al. 2008; Chase et al. 2000; Cui et al. 2006; Davin and de Noblet-Ducoudré 2010; Fan et al. 2015a, b; Feddema et al. 2005; Gero and Pitman 2006; Hoffmann and Jackson 2000; Lee et al. 2011; Li and Smith 2010; Li et al. 2009; Pielke et al.

2007a, b; Puma and Cook 2010; Roy et al. 2007, 2011). It is found that even when we use the same model physical parameters and force by the same atmospheric boundary conditions, different land surface properties can still result in notably different surface fluxes (Chen et al. 2012). Therefore, using more accurate and reliable land cover data can lead to reductions of regional climate model uncertainties (Giorgi et al. 2000). In recent decades, China has experienced significant LCC (Liu et al. 2003). China is one of the largest countries in the world and home of 1.4 billion people with a rapidly expanding economy (United Nations, Department of Economic and Social Affairs, Population Division 2015). In the context of these dynamic socioeconomic conditions (which drives LCC), it is critical that we assess recent LCCs in China and their impacts on climate. However, the quality of the current land cover data used in regional climate models are always not up to date and not accurate, especially for China (Sertel et al. 2010). To this end, land cover data sets from different periods are essential to understand the impacts of LCC on weather and climate. Because land cover data sets may come from different sources as well as with different classification schemes, it is important to investigate the sensitivity of regional climate models to the land cover data sets.

Specifically, the purpose of this study is to investigate the sensitivity of the weather research and forecasting (WRF) model to land cover data sets from three different periods including 1990, 2000, and 2009. Simulations were conducted for three hydroclimatic regimes, which include a wet year (1998), a dry year (2011), and a 'normal' year (2000), as well as year 2001. The WRF model simulation with 2001 LC data set is used as baseline simulation. These LC data sets from different periods also provide an assessment of potential climatic impacts of LCC over the last two decades in China.

The 1990 LC data set was developed from data collected by the advanced very high-resolution radiometer (AVHRR) sensor of the National Oceanographic and Atmospheric Administration (NOAA) satellite. Data sets for later years (2000, 2001, and 2009) were from the moderate-resolution imaging spectroradiometer (MODIS) sensors. Since MODIS data were not available before 2000, AVHRR land cover product was used for the 1990 LC data set. MODIS global land cover classification at 1-km resolution (Friedl et al. 2002), created using data between July and December 2000, was used to represent the Earth's ecosystems in the WRF land surface parameterization scheme. This classification is thought to be composed of higher-quality data than previous sensors and has the most detailed land-use map to date. Validation of MODIS land products is undertaken over a range of conditions. For example, a study by Hansen et al. (2002) shows that MODIS data is a substantial improvement over AVHRR in mapping tree cover. The MODIS land-use map was produced based on a global digital database of land-use type images (e.g., Landsat TM) updated every 16 days. The MODIS land cover supplies an International Geosphere–Biosphere Program (IGBP) land cover classification (Belward et al. 1999; Scepan 1999) with 17 different land cover types, including major natural vegetation types, agricultural land use, and several categories of land surfaces with little or no plant cover (i.e., bare ground, urban areas, and permanent snow and ice). Again, the data from these three periods and two different types of sensors provide two opportunities at the same time: (a) model sensitivity to these data sets and (b) impacts of LCC over the last two decades. One caveat of this investigation is that all three data sets were not from the same satellite platforms. Note that our study focuses on years before 2012, because unavailability of MODIS data after 2012 hindered the investigation of LCC in China over the recent years and the identification of the impacts of these changes on weather and climate.

A limited number of modeling studies have been conducted focusing on LCC in China and their potential impacts on climate (e.g., Fu 2003; Sen et al. 2004; Zhang et al. 2009; Zheng et al. 2002). A few studies were focused on impacts of urbanization on temperature in China (e.g., Yang et al. 2011). On the other hand, a relatively larger number of studies on LCC were conducted based on satellite and other socioeconomic data (Ramankutty and Foley 1998). However, there has been no attempt to use MODIS data for the estimation of LCC in China. Moreover, LCC in China and their impacts on climate need to be improved. Hence, this study links MODIS data-based LCCs and their climatic impacts in China through regional climate modeling.

2 Materials and methods

2.1 Model description

This research is based on the analysis of the model simulations performed by a widely used regional climate model WRF version 3.6.1. The WRF can be used for spatial scales ranging from a few meters to thousands of kilometers and is suitable for both operational forecasting and atmospheric research (Skamarock and Klemp 2008). In this work, the following configuration is used for the experiments: the ARW version of WRF, NOAH land surface model (Chen and Dudhia 2001), the new Kain–Fritsch convective parameterization scheme (Kain 2004), WSM6 (Hong and Lim 2006) microphysics scheme, the Yonsei University counter-gradient boundary layer turbulence transfer scheme (Hong et al. 2006), and the community atmospheric model radiative transfer scheme (Collins et al. 2004).

2.2 Experimental design

In this study, three sets of simulations were conducted for the years 1998, 2000, and 2011. In other words, WRF simulations used the data from these 3 years as the initial and boundary conditions. These years are considered as our experimental simulations (EXP). These 3 years represented a wet (1998), 'normal' (2000), and a dry year (2011) in China. Each set of simulations includes four model runs with data sets of 1990, 2000, 2009, and WRF CTL. For example, for the 1998 surface conditions, simulations with 1990, 2000, and 2009 (Fig. 2c, d) LC data sets and control (CTL) land cover data (2001) (Fig. 2a) constitute one set of experiments. In other words, 12 simulations are conducted for entire China for all three hydroclimatic conditions (i.e., 1998, 2000, and 2011) and three LC data sets (1990, 2000, and 2009) along with CTL simulations (Table 1). CTL LC data for 2001 provided by WRF is used as the default option. The model is integrated over a domain covering the entire area of China with a central point at 37°N and 102.5°E. The horizontal resolution is 30 km with 175 grid points in the east–west direction and 151 grid points in the north–south direction. There were 37 vertical atmospheric levels with the model top at 50 hPa (Fig. 1). The time step is 180 s. Atmospheric lateral boundary conditions and initial atmospheric fields are obtained from ERA-Interim Re-analysis. The WRF runs started at 0000 UTC 1 April and ended at 0000 UTC 1 September for each simulation with the first 2 months treated as spin-up period.

2.3 Land cover data

As noted above, the LC data (1990, 2000, and 2009) for each atmospheric boundary condition (1998, 2000, and 2011) are from the Earth Observation Of Climate Change (EOCC) (http://green.tea.ac.cn/, Hao and Gen-Suo 2012; Hu and Jia 2010). WRF's land-use classifications are given by the US Geological Survey (USGS) global land cover characteristics database with 24 vegetation categories. This land-use data set is derived from 1-km AVHRR data in a 12-month period spanning from April 1992 to March 1993. The goal was to provide long-term LC data sets for climate models to improve the model simulation accuracy and surface parameterization. Multi-source land cover products, including USGS, MODIS land cover data sets and China land use data sets (CLU), derived from satellite platforms are used to investigate in detail the accuracy of land cover classification for land cover data fusion. Three periods (1990, 2000, and 2009) are considered as important turning points for land surface change influenced by human activities over the last decades in China. IGBP land cover classification scheme is adopted in this data set, which is validated by high-resolution images (Landsat TM/ETM+) to ensure its suitability and accuracy with the fraction cover value of each class aggregated from 1-km resolution land cover products. Three levels of spatial scale (3.3, 10, and 30 km) are available to provide nesting input for climate model simulation over China and its main megacity areas with the final format in NetCDF. In this paper, 30-km resolution LC data sets are used. Note, LC data for 1990, 2000, and 2009 is only produced for China; such data for surrounding countries are not available. The LC data for surrounding countries of China are from WRF default MODIS LC data.

The changes in the main physical properties due to the modified land cover types compared to CTL experiments are presented in Figs. 2a–d and 3. Most of the differences among the LC data sets are in transitional zones and mountainous regions. There are fairly good agreements in the plains, deserts, and large areas of croplands. There are 10,242 model grids in total among the territories of China. Compared with the CTL simulation (Fig. 3), 2616 grid

Table 1 Experiment design

EXP sets	EXP name	LC data	Simulation year
WET	W0	CTL LC	1998
	W1	1990 LC	1998
	W2	2000 LC	1998
	W3	2009 LC	1998
NOR	N0	CTL LC	2000
	N1	1990 LC	2000
	N2	2000 LC	2000
	N3	2009 LC	2000
DRY	D0	CTL LC	2011
	D1	1990 LC	2011
	D2	2000 LC	2011
	D3	2009 LC	2011

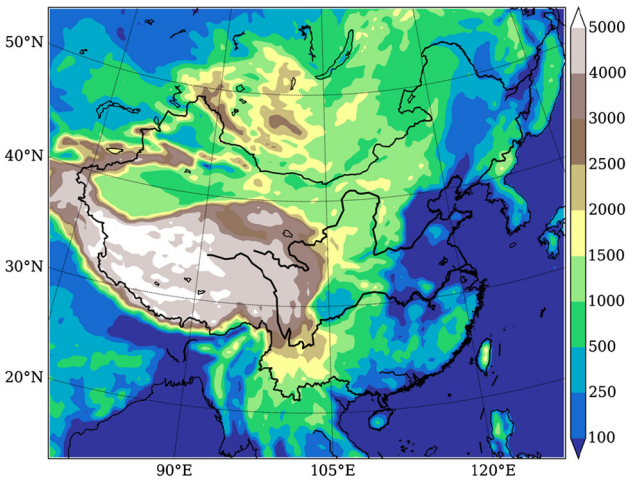

Fig. 1 The WRF model domain and the model topography (units: m)

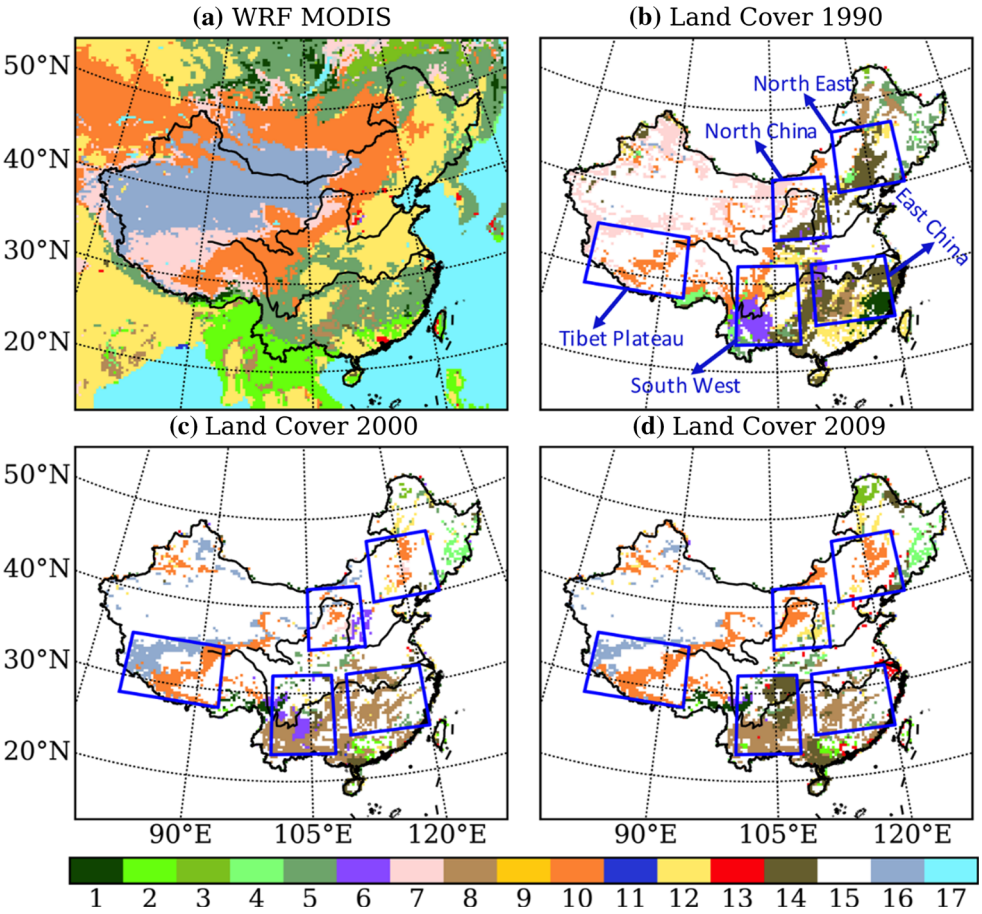

Fig. 2 Land cover/land use maps for each set of the simulation experiments. **a** Vegetation use in the CTL experiments. **b–d** The three new land cover/land use data (1990, 2000, 2009); only grid cells with changes in land cover are shown. *1* Evergreen needleleaf forests. *2* Evergreen broadleaf forests. *3* Deciduous needleleaf forests. *4* Deciduous broadleaf forests. *5* Mixed forests. *6* Closed shrublands. *7* Open shrublands. *8* Woody savannas. *9* Savannas. *10* Grasslands. *11* Permanent wetlands. *12* Cropland. *13* Urban and built-up land. *14* Cropland/Natural vegetation mosaics. *15* Snow and ice. *16* Barren. *17* Water bodies

cells in the 1990 data set are changed to three LC categories, namely evergreen broadleaf, mixed forests, and bare lands. In the 2000 LC data set 2613 grid cells are changed to three land cover categories: mixed forests, open shrublands, and croplands. In the 2009 data set, 2704 grid cells are changed to mixed forests, open shrublands, and croplands.

For the LC data of 1990, the area of bare lands is less than CTL, while the area of croplands is greater. In northeast China, it is very different from the WRF default MODIS data with about 20 % croplands converted to mixed forests, 9 % croplands to the cropland/nature vegetation mosaic, 9.7 % croplands to wooded savanna, and 13 % grasslands to croplands. In other words, there are more trees in the 1990 LC data than the WRF default MODIS data in northeast China. For the LCC data of 2000 and 2009, the main features are the replacement of mixed forests by croplands, and shrublands by grasslands, in southern China. For land cover data in 2000, the pattern of land cover in northeast China is very similar to the WRF default MODIS data, except that about 10 % croplands are changed to grasslands. In east China and southwest China, many areas of mixed forest in the CTL data are changed to woody savannas; in other words, there are fewer trees in

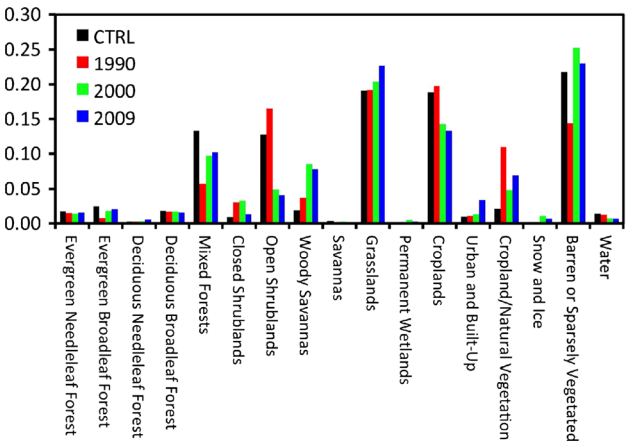

Fig. 3 The fraction of each land cover category for the four LCC datasets (CTL, 1990, 2000, and 2009)

these areas. For the 2009 LC data set, there are more areas of grasslands category in the northeast and even less trees in the southwest, as more mixed forests in CTL are changed to "woody savannas" and "cropland/natural vegetation mosaics". It can be seen from Fig. 3 that most of the LC are under barren and sparsely vegetated cropland and grassland category. In addition, there is a steady increase in

area covered (fractional coverage) by 'barren and sparsely vegetated' and a decrease in cropland category in newer LC data sets (Fig. 3). There is also a significant expansion of urban area in 2009 data set around the megacities of China, especially in the Yangtze River Delta, Pearl River Delta, and Bohai Sea Ring area. This is consistent with the high growth of population and economy, urbanization, and industrialization during 1990–2009 in these regions.

Though the WRF default LC data set is based on MODIS data from 2001, which is very close to the 2000 data set based on multi-sources including MODIS. There are still many noticeable differences in LC categories in southwest China, Tibetan Plateau, and transitional zones between forest and grasslands in the north and northeast. These differences are unlikely from actual changes of LC on the ground, but rather stem from differences in data sources and classification schemes used in these data sets. However, they can make differences in regional climate simulations as different representation of LC in models can alter the land surface–atmosphere interactions.

The ERA-Interim reanalysis from the European Centre for Medium-Range Weather Forecasts (ECMWF), with a 0.7° horizontal resolution, is used for the initial and lateral boundary conditions in all simulations. China monthly surface mean temperature and monthly precipitation 0.5° × 0.5° gridded data sets (available at http://cdc.cma.gov.cn) are used for model validation.

2.4 Methods

To better understand the climatic impacts of LCC and impacts due to different land cover data sets, we have selected five different eco-geographical regions based on the LC changes (Fig. 2). Our discussions will highlight changes in different variables in these regions. The results discussed below are the differences between W1 (W2, W3) and W0; N1 (N2, N3) and N0; and D1 (D2, D3) and D0. As shown in Table 1, W denotes a wet year (1998), N a normal year (2000), and D a dry year (2011). Numbers 0–3 correspond to control run with default WRF LC (0) and three LC data sets from 1990, 2000, and 2009, respectively. The discussion in this paper focuses on the summer seasons (June–August), because they represent growing seasons when land atmosphere interactions are more vigorous. In addition, we have calculated the average results for the simulations for these 3 years (1998, 2000, and 2011) for each of the land cover data sets (1990, 2000, 2009, and 2001). We have also completed the calculations of simulated differences between the averages of 3 years (1998, 2000, 2011) for each land cover data set (1990, 2000, and 2009) and 3 years average for the control land cover data set (2001). The averages of the three hydroclimate regimes somewhat represents long-term climatology, since they include all wet, normal, and dry phases of the system. This approach also allowed us to be computationally efficient.

3 Results

3.1 Evaluation of the control run simulated climate

The model's performance was evaluated in terms of 2-m temperature (T2m) and precipitation in summer. Figure 4 presents the 1998 (wet), 2000 (normal), and 2011 (dry) summer (JJA) average T2m distributions for observations, the model control runs (W0, N0, and D0), and the difference between model control runs and observations. The WRF control simulations reproduce T2m distribution for the three typical simulations in warm seasons with the spatial correlation coefficient of 0.93 with observations. The overall patterns of the observed and model-simulated temperatures bear a resemblance to the observed structure of the northwest–southeast gradients, though the model simulations tend to exceed the observations by 1–2 °C over North China Plains and are colder than observations in south China. Figure 5 presents the 1998 (wet), 2000 (normal), and 2011 (dry) summer (JJA) average precipitation distributions for observations and the model control runs. The simulated summer precipitation in the control runs agree well with the observations, the spatial correlation coefficients for 1998 (wet), 2000 (normal), and 2011 (dry) are 0.66, 0.63, and 0.74. The summertime precipitation field from the CTL simulations can capture the observed large-scale pattern, but the magnitude is underestimated in Yangtze River region and northeast China, but overestimated in south China, in general.

On regional scales, there are some biases in simulated temperature and precipitation relative to observations. Some persistent biases in the simulated temperature and precipitation in the wet, normal, and dry years for CTL simulations seem to co-locate with areas where significant LC differences occur in the newer data sets. The CTL simulation for all years have a negative temperature bias south of Yangtze River where a large area of mixed forest, in the CTL LC data set, is replaced with woody savannas or cropland and natural vegetation mosaic in the experiment data sets. There are also cold biases relative to observation near the northwest brim of the Tibetan Plateau where large areas of open shrublands are replaced by the category of barren land in the 2000 and 2009 data set. In terms of precipitation, it tends to simulate greater precipitation south of Yangtze River for both the wet year (1998) and dry year (2011) in the CTL, with higher precipitation in northeast China for all the years. Both regions see significant LC difference when we compared the CTL LC data set and the newer data sets. In the following section, the

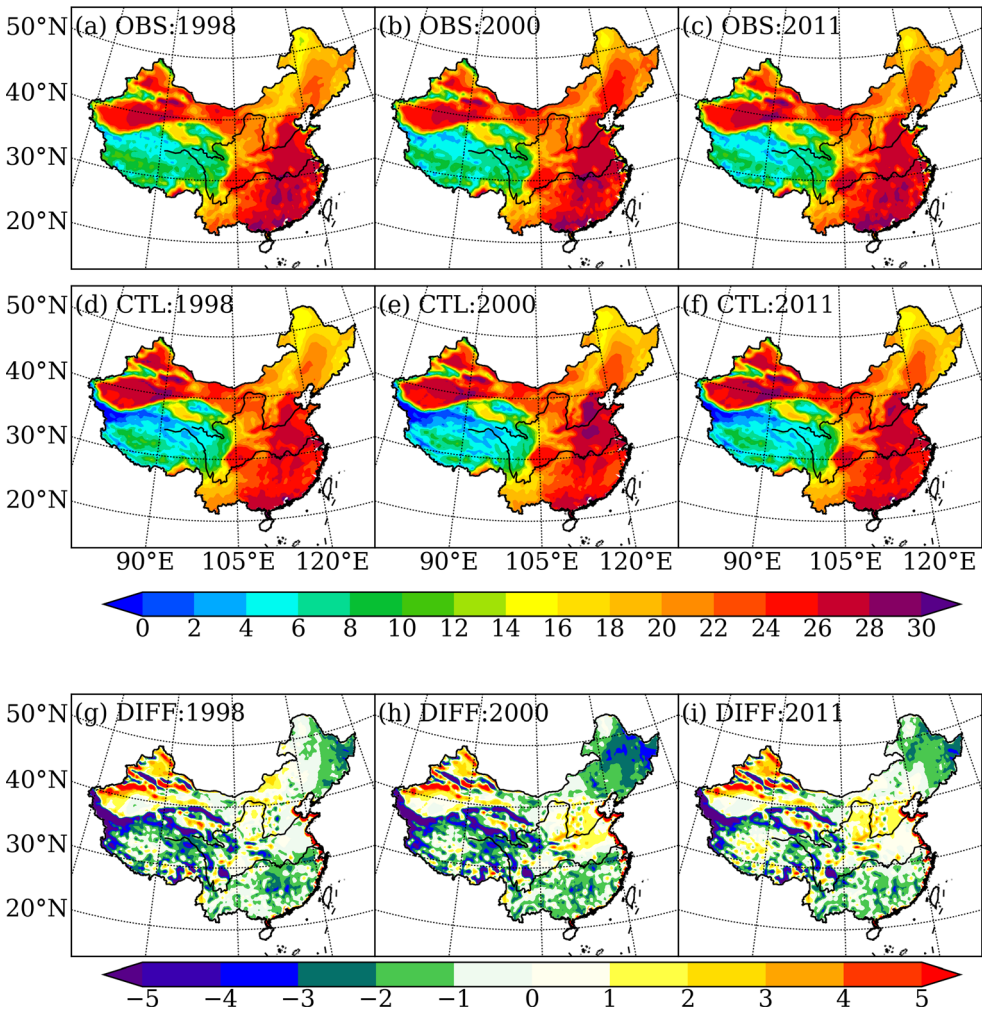

Fig. 4 Mean summer near-surface air temperature (°C) for 1998, 2000, and 2011: **a**–**c** observed, **d**–**f** simulated CTL

improvements in simulation over CTL due to better-validated LC data in several regions are discussed.

3.2 Effects of LCC and LC data sets on temperature and precipitation

The mean differences between the EXP and CTL simulations (e.g., W1 − W0) during wet, normal, and dry summers are analyzed to understand the possible effects of different land cover data on the surface air temperature and precipitation over China (Figs. 6, 7). All three sets of land cover experiments simulate a warmer near-surface summer temperatures in most areas of China, especially in southwest China and south of Yangtze River where large differences of LC exist between EXP and CTL, as mentioned in the last section. For the LCC data in 1990, in the wet year, the decreases of T2m are found in northeast China. In the normal year, the decreases of T2m are found in both the northeast and lower reach of Yellow River areas. But in the dry year, the decreases of T2m shift to only north China. For LCC data in 2000 and 2009, which are very similar to each other, the LCCs have similar effects on regional climate, but with different intensities. Though warming effects are found in most parts of China, especially in south China, the cooling effects were found in the Tibetan Plateau and Yellow River basin, which is possibly related to the land cover changes in these areas in the experiment data sets. For simulations using 2009 LC data sets (W3, N3, D3), the areas with megacities, namely Yangtze River Delta, Pearl River Delta and Bohai Sea Ring area, simulate warmer surface temperatures than CTL and other experimental cases. This may be related to LC representing urban areas in these regions.

The summer precipitation differences for each of the land cover experiments are shown in Fig. 7 and Tables 2, 3, 4. Significant changes in precipitation are found between the LCC experiments and CTL experiment. The largest absolute changes between 54 and 83 mm were found in southeastern China for the summer season. In southeastern China, the main difference in experiment LCs relative to the default land cover is deforestation. Many grid cells are shifted from trees to croplands (1990) and trees to savannas

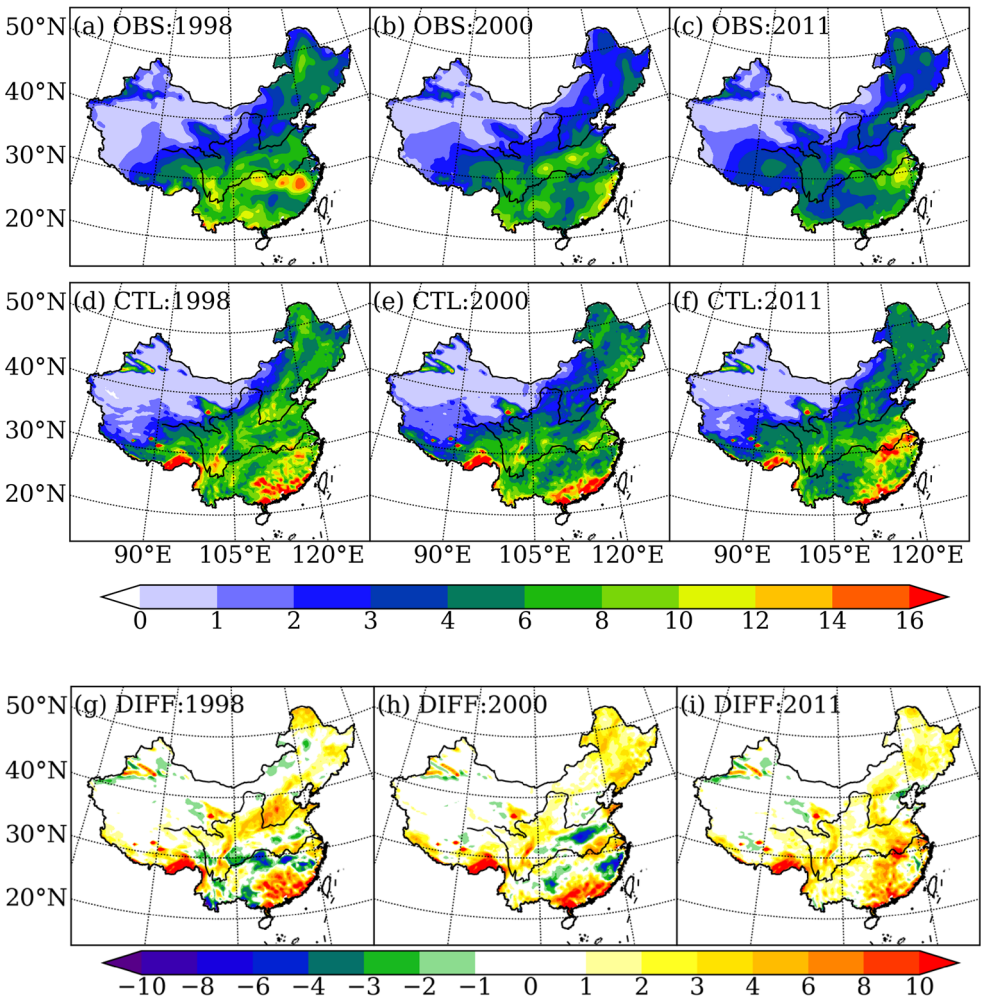

Fig. 5 Mean summer precipitation (mm day^{-1}) for 1998, 2000, and 2011: **a**–**c** observed, **d**–**f** simulated CTL

(2000 and 2009), which cause large changes in roughness length values. Significant changes in precipitation were found in southern China. All three sets of experiments simulated less precipitation than CTL simulations. Forest aerodynamic roughness causes turbulence and enhances the exchange of sensible heat and moisture from the surface to air (Rotenberg and Yakir 2010; Peng et al. 2014). Also, the moisture content above tree-covered areas is larger than cropland/grassland, which could enhance convection, cloud formation, and rainfall. Better representation of the deforestation in southwest China and east China in recent years in the experiment data sets may cause the decrease in simulated precipitation, which is closer to the observed precipitation than CTL.

For the wet year, compared with the observation, CTL simulation has a deficiency of precipitation in the region between the Yellow River and Yangtze River and a positive bias in north China. Compared to W0, W1 simulated more precipitation in the south of Yangtze River and Huaihe River Valley, but for W2 and W3, regions with higher precipitation are found between the Yellow River and Yangtze River region. Relative to W0, less precipitation is simulated for North China Plain for W1, W2 and W3. W1 with 1990 LC data seems to reduce the dry bias around the middle and upper reach of the Yangtze River and Huaihe River. However, W2 with the most up-to-date LC only reduces the dry bias in the CTL in the Huaihe River Valley. Though the 2000 LC is based on measurement close to 1998, there was a significant forestry policy shift in China in the fall of 1998 affecting the region around the upper and middle reaches of Yangtze River. After 1998, the "Grain-for-Green Plan" as a countermeasure for the severe flooding event in 1998 converted large areas of farmlands to forest, especially in the steep terrains of Guizhou and Sichuan Provinces. Due to the sudden change in afforestation trend in the region around 1998, the 2000 LC may not be a better representation of LC in 1998 (compared to the 1990 LC).

For the normal year, CTL simulation produced less precipitation over the Huaihe River Valley and southeast China compared to observation and more precipitation in the eastern part of southwest China. For N1, less precipitation is

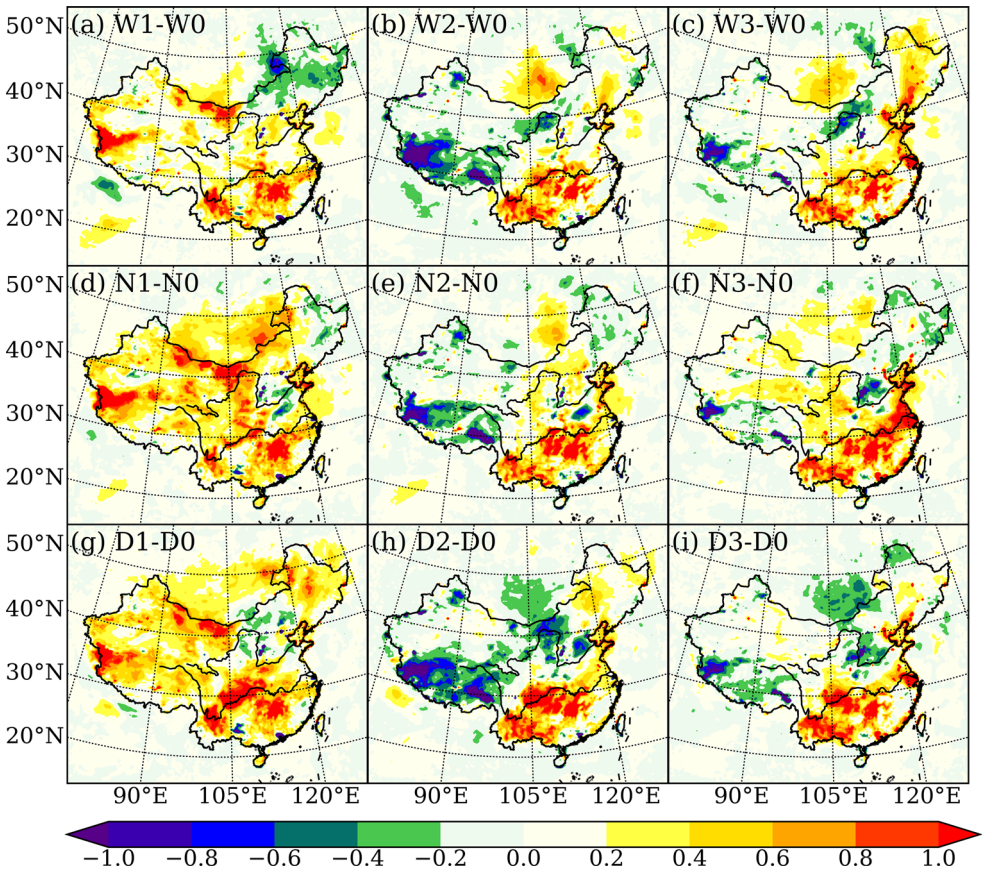

Fig. 6 Spatial changes (LCC-CTL) of near-surface air temperature (°C) for the three simulated years 1998, 2000, and 2011 for summer (JJA): **a** W1 − W0, **b** W2 − W0, **c** W3 − W0, **d** N1 − N0, **e** N2 − N0, **f** N3 − N0, **g** D1 − D0, **h** D2 − D0, **i** D3 − D0

found in the south of the Yangtze River, in eastern part of southwest China and the southeast coast; higher precipitation is simulated in north China, Huaihe River Valley, and upper reach of Yellow River. For N2 and N3, less precipitation is simulated in the Yangtze River region and south China and higher precipitation is found in the Huaihe River Valley, coastal area of southeast China, and Bohai Sea Ring area. Compared with N1, N2 with the most up-to-date LC produced much improved precipitation distribution pattern in southwest China and Tibetan Plateau where significant LC changes occurred between 1990 and 2000.

For the dry year, the spatial distribution of the precipitation difference is similar to that of the normal year. CTL simulation overestimates the precipitation in south China compared to the observation. For D1, higher precipitation is estimated to the south of Yangtze River, especially in the eastern part of southwest China and southeast China. For D2 and D3, greater precipitation is found in southeast China, whereas less precipitation is found in other areas to the south of Yangtze River. Though the precipitation patterns of D2 and D3 are similar, D3 as the most recent LC data set for 2011 produced better temperature simulation in the megacity areas where large LC changes occurred due to the rapid urban expansion during the first decade of the twenty-first century.

3.3 Effects of LCC and LC data sets on energy budget and circulation

Figure 8 shows the spatial changes of the surface energy budget in the summer of the normal year 2000. For the LCC data in 1990, the replacement of bare soil by savannas and savannas by grasslands in the western Tibetan Plateau caused the sensible heat flux (SH) to increase in this area for summer compared to the WRF default MODIS land cover data. In east China, replacement of mixed forests by crops caused the SH to significantly decrease in north China and south of Yangtze River and to increase in the Yellow River region (Fig. 8d).

For the LCC data in 2000 and 2009, the two land cover data sets seem very similar except that the urban areas expanded in 2009. Compared to the default land cover data, in the western part of the Tibetan Plateau, a replacement of savannas by bare soil and grasslands by bare soil also causes the SH to increase significantly. Besides this change, SH in most of China decreased, especially in northeast, Bohai Sea Ring Area, and Pearl River Delta Region (Fig. 8b, c). The changes in latent heat flux (LH) show the opposite pattern of SH changes in these areas with LC changes (Fig. 8). The albedo increases in southwest and south China led to higher SH and lower LH. In

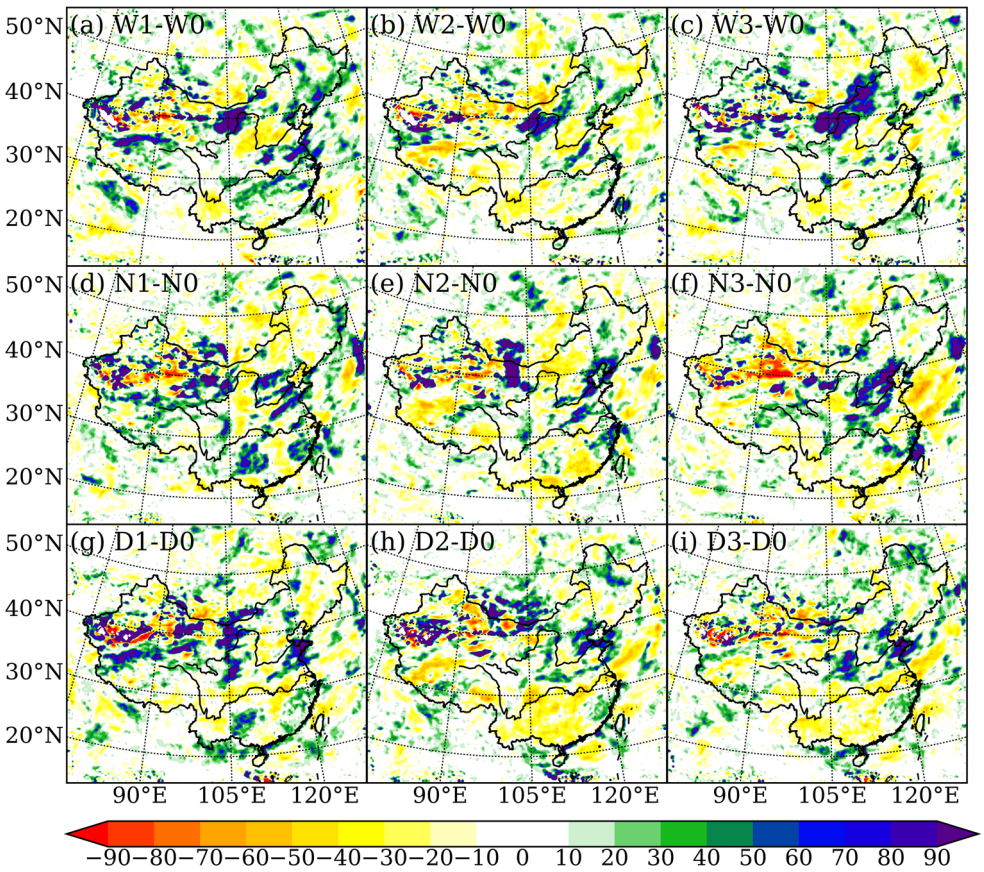

Fig. 7 Spatial changes (LCC-CTL) of precipitation (%) for the three simulated years 1998, 2000, and 2011 for summer (JJA): **a** W1 − W0, **b** W2 − W0, **c** W3 − W0, **d** N1 − N0, **e** N2 − N0, **f** N3 − N0, **g** D1 − D0, **h** D2 − D0, **i** D3 − D0

most areas of China, LH increases. It is especially noticeable in the eastern part of China due to the significant changes in LC. The replacement of mixed forests by woody savannas, croplands, and urban areas over the southern China and expansion of grasslands and croplands in the northern and northeastern China has resulted in higher partition of energy into SH. Over the Tibetan Plateau, SH increases steadily for the newer data sets. Overall, considering the differences in SH over the Tibetan Plateau, north and northeastern China, most noticeable changes in SH are found in simulations for the 2000 and 2009 data sets, which suggests they are caused by the land cover changes. Lower SH compared to CTL in some regions in the experiments also results in more energy to be partitioned into LH. For example, some areas of northern China experienced up to 25 W m^{-2} higher LH compared to N0 for N2 and N3 (Fig. 8c, g, k). Overall, it is evident that due to LCC and the use of associated LC data sets, changes in LH is more widespread compared to the CTL for some areas of northern China.

Though it is difficult to separate climate regime's impact and LC data's impact, the magnitude of the differences in SH and LH between different LC data sets and CTL data set for the normal year of 2000 suggests that northeastern, north China, and lower–middle reaches of the Yangtze River regions are more sensitive to the 2000 LC data set. On the other hand, the magnitude of the differences in SH and LH suggests that the southwest, sorthwest, and Tibetan Plateau regions are more sensitive to 2009 LC data sets during summer season where we see many changes in land cover compared with the default WRF LC data set.

The results from the experimental simulations for the normal year show that higher SH in many areas, particularly over northern China, southwest China, south of Yangtze River in east China, and Tibetan Plateau, compared to the CTL. Expansion of grasslands in the Tibetan Plateau and increase of urban areas, woody savannas, and closed shrublands in the north China influenced energy partitioning and increased SH. Comparison of LC data sets suggest that expansion of croplands in northeast results in reduced SH. In the upper reaches of Yellow River, which is relatively closer to the desert areas, both shrublands and croplands (irrigated) can be found. As expected for the heat flux changes induced by changes in the vegetation cover, regions of higher and lower SH experienced lower and higher LH, respectively.

In terms of net radiation (NR), in north China, east China and northeast China, where plains and cropland dominate, the differences are the least between W2 and W0, N2 and N0. This is consistent with the fact that

Table 2 Differences [experiment (EXP) − control (CTL)] in fluxes, temperature, and precipitation for a wet year (1998) for five regions of China (see Fig. 1)

Differences	1998 summer (JJA)				
	RN	SH	LH	T2 m	PR
Northeast					
W1 − W0	1.19	0.37	3.01	−0.2	21.5
W2 − W0	0.33	1.42	−1.24	0.1	13.5
W3 − W0	7.27	3.78	0.52	0.4	6.1
North China					
W1 − W0	3.47	0.98	4.46	0.3	−21.2
W2 − W0	0.46	2.94	2.83	−0.1	3.4
W3 − W0	1.61	0.83	5.49	−0.1	12.9
East China					
W1 − W0	4.19	2.28	−1.41	0.5	34.1
W2 − W0	0.01	3.38	−9.85	0.3	1.5
W3 − W0	7.91	5.51	−4.23	0.4	−15.8
Southwest					
W1 − W0	0.03	1.93	−3.30	0.4	−4.8
W2 − W0	1.46	3.23	−6.27	0.3	−35.9
W3 − W0	1.34	3.18	−6.19	0.3	−19.0
Tibetan Plateau					
W1 − W0	0.84	−0.91	−2.81	0.2	−1.4
W2 − W0	4.03	−0.67	−3.23	−0.6	−9.8
W3 − W0	3.11	−0.35	−1.78	−0.4	−4.3

Calculations are based on land cover datasets from three periods, including, 1990, 2000, and 2009. The WRF-provided default land cover dataset for 2001 was used as CTL

RN net radiation (W m^{-2}), *SH* sensible heat flux (W m^{-2}), *LH* latent heat flux (W m^{-2}), *T2m* two-meter temperature (°C), and *PR* precipitation (mm)

Table 3 Differences [experiment (EXP) – control (CTL)] in fluxes, temperature, and precipitation for normal year (2000) for five regions of China (see Fig. 1)

Differences	2000 Summer (JJA)				
	RN	SH	LH	T2m	PR
Northeast					
N1 − N0	26.24	7.30	14.56	1.6	−47.6
N2 − N0	18.91	5.33	10.10	1.2	−12.3
N3 − N0	20.60	5.39	9.14	1.3	−23.3
North China					
N1 − N0	2.77	4.94	−0.46	0.9	−37.5
N2 − N0	1.70	2.82	−2.88	0.5	−43.8
N3 − N0	5.87	4.99	2.48	0.5	−24.5
East China					
N1 − N0	12.33	10.04	−3.03	0.3	−53.6
N2 − N0	9.73	12.07	−10.48	0.2	−82.5
N3 − N0	16.32	12.98	−4.46	0.4	−61.6
Southwest					
N1 − N0	0.27	2.20	−4.07	−0.4	2.5
N2 − N0	1.05	2.80	−7.29	−0.6	−22.6
N3 − N0	2.18	2.52	−5.44	−0.5	−29.6
Tibetan Plateau					
N1 − N0	1.09	0.73	−2.26	−0.2	9.4
N2 − N0	1.25	0.29	−2.74	−1.0	−9.7
N3 − N0	1.84	1.08	−1.00	−0.8	−1.7

Calculations are based on land cover datasets from three periods, including, 1990, 2000, and 2009. The WRF-provided default land cover datset for 2001 was used as CTL

RN net radiation (W m^{-2}), *SH* sensible heat flux (W m^{-2}), *LH* latent heat flux (W m^{-2}), *T2m* two-meter temperature (°C), and *PR* precipitation (mm)

satellite-based LC data sets agree well with multi-source LC data sets in these LC types and these 2 years are very close to each other.

There are large differences between 2000 LC and CTL (MODIS 2001) in southwest China, south China, and Tibetan Plateau even though these two data sets are very close to each other in time. The 2000 LC data set are compiled with multiple sources including in situ and ground validation. In transitional zones and regions with topography, the differences between 2000 LC and CTL are large (Fig. 2). Therefore, the differences of simulated LH, SH, NR, temperature, and precipitation are not always smallest between these two data sets, especially in the transitional zones and mountainous regions.

Figure 9 shows the 850 hPa wind field and geopotential height changes in summer for the three sets of simulations. We focus on lower atmospheric geopotential height, because we are interested in determining the direct effects of the LC data sets on the lower atmosphere. For the wet year, compared to W0, there is a cyclonic wind anomaly over eastern China for W1. The anomalous winds indicate a strengthened summer monsoon over eastern China, which contributes to the increased precipitation over east China and northeastern China. For W2 and W3, there are very minor anticyclonic wind anomalies over northeastern China, which might contribute to the reduced precipitation over northern and northeastern China. For the normal year, the N1 and N3 LC data sets simulations show anticyclonic wind anomalies over northeastern China. Other than the above common features, several anomalies are also found for N1 and N3: a cyclonic wind anomaly for N1 over southern China; a cyclonic wind anomaly for N3 over Bohai Sea Ring Area and Pearl River Delta Region; and an anticyclonic wind anomaly for N3 over east China and south China. For the dry year, D1 shows an anticyclonic wind anomaly over northeastern China, while D2 and D3 show an anticyclonic wind anomaly over southern China and a cyclonic wind anomaly over northeastern China.

Table 4 Differences [experiment (EXP) –control (CTL)] in fluxes, temperature, and precipitation for dry year (2011) for five regions of China (see Fig. 1).

Differences	2011 Summer (JJA)				
	RN	SH	LH	T2m	PR
Northeast					
D1 − D0	27.11	0.71	14.56	0.3	−6.3
D2 − D0	22.62	−1.57	10.10	0.3	−6.7
D3 − D0	27.03	2.34	9.14	0.3	−0.3
North China					
D1 − D0	1.80	2.22	−0.46	−0.0	1.0
D2 − D0	−0.87	−0.83	−2.88	−0.4	3.7
D3 − D0	3.58	2.28	2.48	−0.2	6.8
East China					
D1 − D0	0.58	7.20	−3.03	0.5	−30.0
D2 − D0	−2.17	6.64	−10.48	0.3	-42.9
D3 − D0	2.05	8.41	−4.46	0.3	−37.9
Southwest					
D1 − D0	4.12	1.76	−4.07	0.7	−9.0
D2 − D0	4.02	3.45	−7.29	0.4	−34.9
D3 − D0	5.14	3.42	−5.44	0.4	−26.8
Tibetan Plateau					
D1 − D0	2.51	−0.95	−2.26	0.2	−4.3
D2 − D0	3.88	−1.34	−2.74	−0.7	−6.5
D3 − D0	4.49	−0.45	−1.00	−0.4	−1.6

Calculations are based on land cover datasets from three periods, including, 1990, 2000, and 2009. The WRF-provided default land cover datset for 2001 was used as CTL

RN net radiation (W m^{-2}), *SH* sensible heat flux (W m^{-2}), *LH* latent heat flux (W m^{-2}), *T2m* two-meter temperature (°C), and *PR* precipitation (mm)

These wind anomalies were consistent with the precipitation and temperature changes as higher precipitation lowers surface temperature by decreasing insolation and increasing evaporative cooling (Figs. 6, 7). The spatial distributions of the geopotential height anomalies at 850 hPa are also consistent with the wind fields.

4 Summary and discussion

A regional climate model, the WRF, is used to examine how the new LC data could potentially affect near-surface energy fluxes, temperature, and precipitation over the entire China domain. Three new land cover data sets (LC data in 1990, 2000, and 2009) were used for this study. Compared to the WRF default MODIS LC data, there are more forests in 1990 LC data in northeastern China. In the newer data sets (2000, 2009), there is a steady increase in the area covered (fractional coverage) by 'barren and sparsely vegetated' and cropland category. Many areas of mixed forest in the WRF default LC data set in southwest China and south of the Yangtze River are replaced by woody savannas in the new LC data sets. In central Tibetan Plateau, open shrublands are replaced with grasslands in all of the new data sets. In the northwestern part of the Tibetan Plateau, open shrublands are replaced with barren land in the new data sets of 2000 and 2009. All of these changes are collocated with changes in simulated surface temperature, precipitation, and fluxes in the experiments with the new LC data sets.

Three periods were selected to represent a wet (1998), a normal (2000) and a dry year (2011) for China. The CTL simulations for all the years agree well with the observation in large-scale patterns. However, there are some regional-scale differences noted in temperature and precipitation. There is a consistent cold bias for all hydroclimatic regimes to the south of the Yangtze River and southwest China and in the northwest of the Tibetan Plateau. Higher precipitation was simulated in the central part of east China (south of the Yangtze River).

The experiments with new LC data sets show differences in temperature, precipitation, and energy fluxes compared with CTL simulations in regional scales. Because climate system is complex and non-linear, small change in initial or boundary condition can result in drift from the mean condition. Due to complexity of interactions, at this point it is difficult to discern which difference is directly related to LC changes. Such assessment would require a separate study beyond the scope of this research. However, some of the differences are co-located with regions with significant LC changes and strongly suggest an improvement over CTL simulation. For example, in the new LC data sets, southwest China and the region to the south of the Yangtze River see large areas of mixed forest replaced by woody savannah compared with CTL LC data set, which is consistent with higher surface temperature and less precipitation in the experiment simulations for all years. Compared to CTL, experiments with new LC data sets improved temperature and precipitation simulation, as the new LC data sets are more accurate because of integration of remote sensing data and ground reference [Hu and Jia 2010). Using newer data sets also reduces the temperature and precipitation bias in the northwest Tibetan Plateau where significant LC changes between CTL and experiment data sets. The urbanization in China's three megacity areas over the Yangtze River Delta, Pearl River Delta, and Bohai Sea Ring are captured by the LC difference between 2009 LC and other data sets. Correspondingly, all simulations using the 2009 data set simulate warmer surface temperature in these regions than its counterparts using other LC data sets. The expansion of croplands in northeast resulted in reduced SH. The northeastern and north China and the lower–middle reaches of

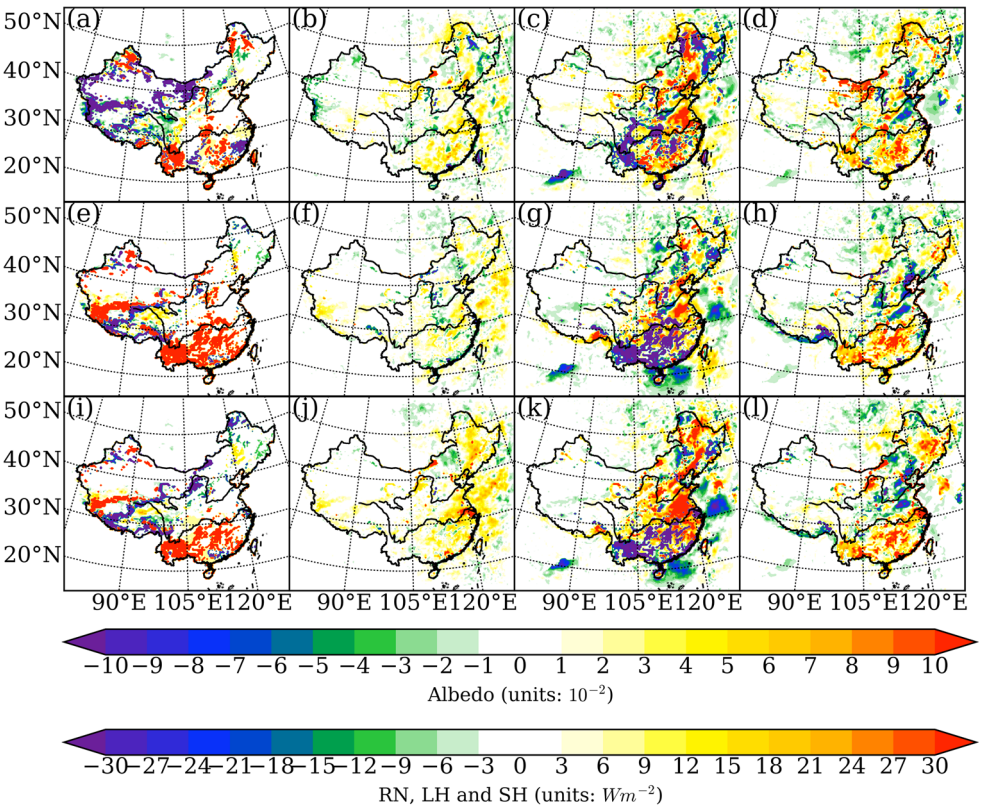

Fig. 8 Spatial changes in summer (JJA) for a normal year (2000): **a** the surface albedo (units: 10^{-2}) changes (N1 − N0), **b** the net radiation (units: W m^{-2}) changes (N1 − N0), **c** the surface latent heat flux (units: W m^{-2}) changes (N1 − N0), **d** the sensible heat flux (units: W m^{-2}) changes (N1 − N0); **e** same as **a** but for (N2 − N0), **f** same as **b** but for (N2 − N0), **g** same as **c** but for (N2 − N0), **h** same as **d** but for (N2 − N0); **i** same as **a** but for (N3 − N0), **j** same as **b** but for (N3 − N0), **k** same as **c** but for (N3 − N0), **l** same as **d** but for (N3 − N0)

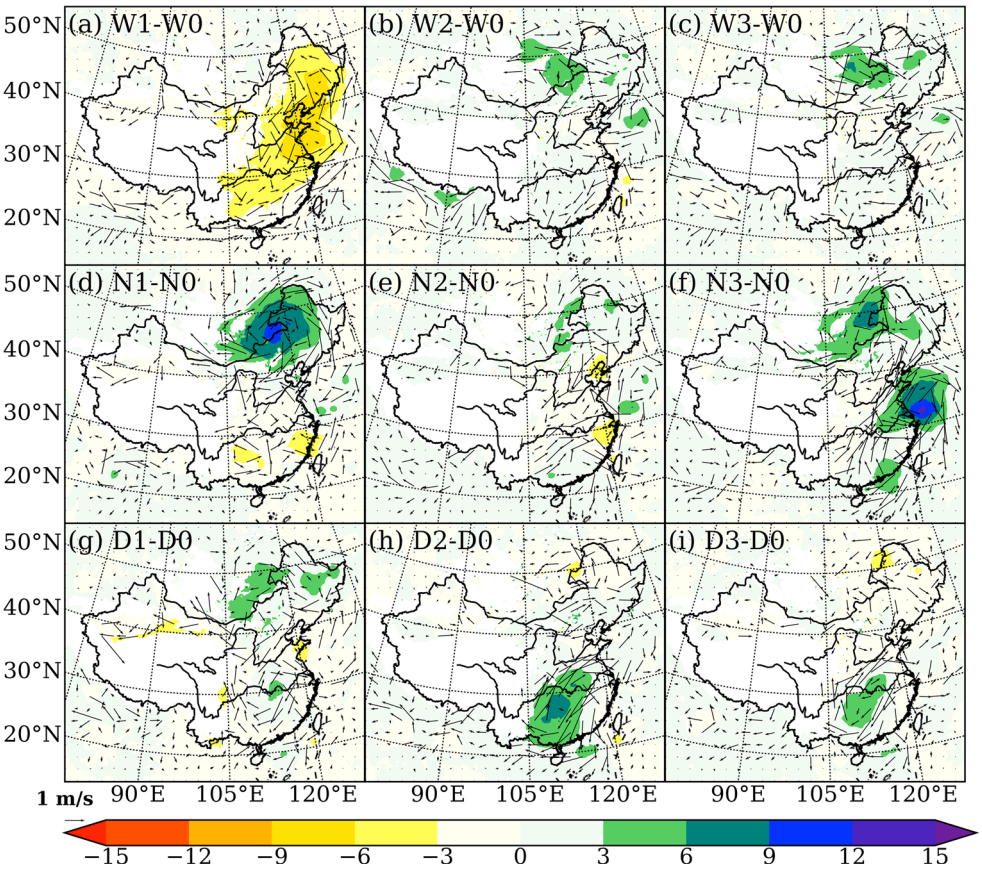

Fig. 9 Spatial patterns of the changes (LCC-CTL) in wind vectors (units: m s^{-1}) and geopotential height (units: geopotential meter) at 850 hPa in summer (JJA)

the Yangtze River regions are more sensitive to the 2000 LC data set, while the southwestern, northwestern, and Tibetan Plateau regions are more sensitive to the 2009 LC data set during summer. The changes of near-surface fluxes then lead to changes in near-surface temperature.

As demonstrated by numerous previous research by others and result presented in this paper, regional weather and climate are highly sensitive to LCC. The large changes in LC due to the fast-paced socioeconomic transformation in China during recent decades require realistic LC datasets to simulate the regional climate change. The first stage of future work is to conduct decadal climate simulation using latest realistic LCC when these datasets are available for the past 30 years. In the background of global climate change, the corresponding LCC will also greatly affect the regional climate in China. The next stages of future research will be directed toward regional climate projection/downscaling using future LC datasets.

Acknowledgments This study was supported by the National Key Basic Research Program of China (Grant No. 2012CB956203), and the National Natural Science Foundation of China (Grant No. 41305062). L. Chen, Y. Li gratefully acknowledges the support from the Global Institute of Water Security at the University of Saskatchewan.

References

Abiodun B, Pal J, Afiesimama E, Gutowski W, Adedoyin A (2008) Simulation of West African monsoon using RegCM3 part II: impacts of deforestation and desertification. Theor Appl Climatol 93(3–4):245–261

Barlage M, Zeng X (2004) The effects of observed fractional vegetation cover on the land surface climatology of the community land model. J Hydrometeorol 5(5):823–830

Beljaars AC, Miller MJ, Viterbo PA (1996) The land surface–atmosphere interaction: a review based on observational and global modeling perspectives. J Geophys Res 101:7209–7225

Beltrán-Przekurat A, Pielke RA, Peters DP, Snyder KA, Rango A (2008) Modeling the effects of historical vegetation change on near-surface atmosphere in the northern Chihuahuan Desert. J Arid Environ 72(10):1897–1910

Belward AS, Estes JE, Kline KD (1999) The IGBP-DIS global 1-km land-cover data set DISCover: a project overview. Photogramm Eng Remote Sens 65(9):1013–1020

Chang J-T, Wetzel PJ (1991) Effects of spatial variations of soil moisture and vegetation on the evolution of a prestorm environment: a numerical case study. Mon Weather Rev 119(6):1368–1390

Chase T, Pielke R Sr, Kittel T, Nemani R, Running S (2000) Simulated impacts of historical land cover changes on global climate in northern winter. Clim Dyn 16(2–3):93–105

Chen F, Avissar R (1994) Impact of land-surface moisture variability on local shallow convective cumulus and precipitation in large-scale models. J Appl Meteorol 33(12):1382–1401

Chen F, Dudhia J (2001) Coupling an advanced land surface-hydrology model with the Penn State-NCAR MM5 modeling system. Part I: model implementation and sensitivity. Mon Weather Rev 129(4):569–585

Chen L, Ma ZG, Fan XG (2012) A comparative study of two land surface schemes in WRF model over Eastern China. J Trop Meteorol 18(4):445–456

Clark CA, Arritt PW (1995) Numerical simulations of the effect of soil moisture and vegetation cover on the development of deep convection. J Appl Meteorol 34(9):2029–2045

Collins WD, Rasch PJ, Boville BA, Hack JJ, McCaa JR, Williamson DL, Kiehl JT, Briegleb B, Bitz C, Lin S (2004) Description of the NCAR community atmosphere model (CAM 3.0), edited, Technical Note TN-464+ STR, National Center for Atmospheric Research, Boulder, CO

Cui X, Graf HF, Langmann B, Chen W, Huang R (2006) Climate impacts of anthropogenic land use changes on the Tibetan Plateau. Glob Planet Chang 54(1):33–56

Davin EL, de Noblet-Ducoudré N (2010) Climatic impact of global-scale deforestation: radiative versus nonradiative processes. J Clim 23(1):97–112

Fan X, Ma Z, Yang Q, Han Y, Mahmood R, Zheng Z (2015a) Land use/land cover changes and regional climate over the Loess Plateau during 2001–2009—part I. Observed evidences. Clim Chang 129:427–440. doi:10.1007/s10584-014-1069-4

Fan X, Ma Z, Yang Q, Han Y, Mahmood R (2015b) Land use/land cover changes and regional climate overthe Loess Plateau during 2001–2009—part II. Interrelationship from observations. Clim Chang 129:441–455. doi:10.1007/s10584-014-1068-5

Feddema JJ, Oleson KW, Bonan GB, Mearns LO, Buja LE, Meehl GA, Washington WM (2005) The importance of land-cover change in simulating future climates. Science 310(5754):1674–1678. doi:10.1126/science.1118160

Friedl MA, McIver DK, Hodges JC, Zhang X, Muchoney D, Strahler AH, Woodcock CE, Gopal S, Schneider A, Cooper A (2002) Global land cover mapping from MODIS: algorithms and early results. Remote Sens Environ 83(1):287–302

Fu C (2003) Potential impacts of human-induced land cover change on East Asia monsoon. Glob Planet Chang 37(3):219–229

Gero A, Pitman A (2006) The impact of land cover change on a simulated storm event in the Sydney basin. J Appl Meteorol Climatol 45(2):283–300

Giorgi F, Francisco R (2000) Evaluating uncertainties in the prediction of regional climate change. Geophys Res Let 27(9):1295–1298

Hansen M, DeFries R, Townshend J, Sohlberg R, Dimiceli C, Carroll M (2002) Towards an operational MODIS continuous field of percent tree cover algorithm: examples using AVHRR and MODIS data. Remote Sens Environ 83(1):303–319

Hao G, Gen-Suo J (2012) Spatial and quantitative comparison of satellite-derived land cover products over China. Atmos Ocean Sci Lett 5(5):426–434

Hoffmann WA, Jackson RB (2000) Vegetation-climate feedbacks in the conversion of tropical savanna to grassland. J Clim 13(9):1593–1602

Hong S-Y, Lim J-OJ (2006) The WRF single-moment 6-class microphysics scheme (WSM6). Asia Pac J Atmos Sci 42(2):129–151

Hong S-Y, Noh Y, Dudhia J (2006) A new vertical diffusion package with an explicit treatment of entrainment processes. Mon Weather Rev 134(9):2318–2341

Hu Y, Jia G (2010) Influence of land use change on urban heat island derived from multi-sensor data. Int J Climatol 30(9):1382–1395

Kain JS (2004) The Kain-Fritsch convective parameterization: an update. J Appl Meteorol 43(1):170–181

Lee E, Sacks WJ, Chase TN, Foley JA (2011) Simulated impacts of irrigation on the atmospheric circulation over Asia. J Geophys Res Atmos (1984–2012) 116(D8):D08114. doi:10.1029/2010JD014740

Li Y, Smith RB (2010) Observation and theory of the diurnal continental thermal tide. J Atmos Sci 67(9):2752–2765
Li Y, Smith RB, Grubišic V (2009) Using surface pressure variations to categorize diurnal valley circulations: experiments in Owens Valley. Mon Weather Rev 137(6):1753–1769
Liu J, Zhuang D, Luo D, Xiao X-M (2003) Land-cover classification of China: integrated analysis of AVHRR imagery and geophysical data. Int J Remote Sens 24(12):2485–2500
Mahmood R, Hubbard KG (2002) Anthropogenic land-use change in the North American tall grass-short grass transition and modification of near-surface hydrologic cycle. Clim Res 21(1):83–90
Mahmood R, Pielke RA Sr, Hubbard KG, Niyogi D, Bonan G, Lawrence P, McNider R, McAlpine C, Etter A, Gameda S, Qian B, Carleton A, Beltran-Przekurat A, Chase T, Quintanar AI, Adegoke JO, Vezhapparambu S, Conner G, Ase S, Sertel E, Legates DR, Wu Y, Hale R, Frauenfeld QW, Watts A, Shepherd M, Mitra C, Anantharaj VG, Fall S, Lund R, Treviño A, Blanken P, Du J, Chang H, Leeper R, Nair US, Dobler S, Deo R, Syktus J (2010) Impacts of land use/land cover change on climate and future research priorities. Bull Am Meteorol Soc 91(1):37–46
Mahmood R, Leeper R, Quintanar AI (2011) Sensitivity of planetary boundary layer atmosphere to historical and future changes of land use/land cover, vegetation fraction, and soil moisture in Western Kentucky, USA. Glob Planet Chang 78(1):36–53
Mahmood R, Pielke RA Sr, Hubbard KG, Niyogi D, Dirmeyer P, McAlpine C, Carleton A, Hale R, Gameda S, Beltran-Przekurat A, Baker B, McNider R, Legates DR, Shepherd M, Du J, Blanken P, Frauenfeld OW, Nair US, Fall S (2014) Land cover changes and their biogeophysical effects on climate. Int J Climatol 34:929–953. doi:10.1002/joc.3736
McPherson RA (2007) A review of vegetation—atmosphere interactions and their influences on mesoscale phenomena. Prog Phys Geogr 31(3):261–285
Ookouchi Y, Segal M, Kessler R, Pielke R (1984) Evaluation of soil moisture effects on the generation and modification of mesoscale circulations. Mon Weather Rev 112(11):2281–2292
Peng SS, Piao S, Zeng Z, Ciais P, Zhou L, Li LZX et al (2014) Afforestation in China cools local land surface temperature. Proc Natl Acad Sci 111(8):2915–2919. doi:10.1073/pnas.1315126111
Pielke RA (2001) Influence of the spatial distribution of vegetation and soils on the prediction of cumulus convective rainfall. Rev Geophys 39(2):151–177
Pielke R, Adegoke J, Beltran-Przekurat A, Hiemstra C, Lin J, Nair U, Niyogi D, Nobis T (2007a) An overview of regional land-use and land-cover impacts on rainfall. Tellus B 59(3):587–601
Pielke RA, Adegoke JO, Chase TN, Marshall CH, Matsui T, Niyogi D (2007b) A new paradigm for assessing the role of agriculture in the climate system and in climate change. Agric For Meteorol 142(2):234–254
Puma M, Cook B (2010) Effects of irrigation on global climate during the 20th century. J Geophys Res Atmos (1984–2012) 115(D16):D16120. doi:10.1029/2010JD014122
Ramankutty N, Foley JA (1998) Characterizing patterns of global land use: an analysis of global croplands data. Glob Biogeochem Cycles 12(4):667–686
Rotenberg E, Yakir D (2010) Contribution of semi-arid forests to the climate system. Science 327(5964):451–454. doi:10.1126/science.1179998
Roy SS, Mahmood R, Niyogi D, Lei M, Foster SA, Hubbard KG, Douglas E, Pielke R (2007) Impacts of the agricultural Green Revolution–induced land use changes on air temperatures in India. J Geophys Res Atmos (1984–2012) 112(D21):D21108. doi:10.1029/2007JD008834
Roy SS, Mahmood R, Quintanar AI, Gonzalez A (2011) Impacts of irrigation on dry season precipitation in India. Theor Appl Climatol 104(1–2):193–207
Scepan J (1999) Thematic validation of high-resolution global land-cover data sets. Photogramm Eng Remote Sens 65(9):1051–1060
Sen OL, Wang B, Wang YQ (2004) Impacts of re-greening the desertified lands in northwestern China: implications from a regional climate model experiment. J Meteorol Soc Jpn 82(6):1679–1693. doi:10.2151/jmsj.82.1679
Sertel E, Robock A, Ormeci C (2010) Impacts of land cover data quality on regional climate simulations. Int J Climatol 30(13):1942–1953
Skamarock WC, Klemp JB (2008) A time-split nonhydrostatic atmospheric model for weather research and forecasting applications. J Comput Phys 227(7):3465–3485
United Nations, Department of Economic and Social Affairs, Population Division (2015). World Population Prospects: The 2015 Revision, Key Findings and Advance Tables. Working Paper No. ESA/P/WP.241
Yang X, Hou Y, Chen B (2011) Observed surface warming induced by urbanization in east China. J Geophys Res Atmos (1984–2012) 116(D14):D14113. doi:10.1029/2010JD015452
Zhang H, Gao X, Li Y (2009) Climate impacts of land-use change in China and its uncertainty in a global model simulation. Clim Dyn 32(4):473–494
Zheng Y, Yu G, Qian Y, Miao M, Zeng X, Liu H (2002) Simulations of regional climatic effects of vegetation change in China. Q J R Meteorol Soc 128(584):2089–2114